

# CodeBrain: Impute Any Brain MRI via Instance-specific Scalar-quantized Codes

Yicheng Wu<sup>1</sup>(✉), Tao Song<sup>2</sup>, Zhonghua Wu<sup>3</sup>, Zongyuan Ge<sup>1</sup>, Zhaolin Chen<sup>1</sup>, and Jianfei Cai<sup>1</sup>  
<sup>1</sup>Monash University, Clayton, Australia  
<sup>2</sup>Fudan University, Shanghai, China  
<sup>3</sup>Nanyang Technological University, Singapore, Singapore

## Abstract

MRI imputation aims to synthesize the missing modality from one or more available ones, which is highly desirable since it reduces scanning costs and delivers comprehensive MRI information to enhance clinical diagnosis. In this paper, we propose a unified model, **CodeBrain**, designed to adapt to various brain MRI imputation scenarios. The core design lies in casting various inter-modality transformations as a full-modality code prediction task. To this end, CodeBrain is trained in two stages: **Reconstruction** and **Code Prediction**. First, in the Reconstruction stage, we reconstruct each MRI modality, which is mapped into a shared latent space followed by a scalar quantization. Since such quantization is lossy and the code is low dimensional, another MRI modality belonging to the same subject is randomly selected to generate common features to supplement the code and boost the target reconstruction. In the second stage, we train another encoder by a customized grading loss to predict the full-modality codes from randomly masked MRI samples, supervised by the corresponding quantized codes generated from the first stage. In this way, the inter-modality transformation is achieved by mapping the instance-specific codes in a finite scalar space. We evaluated the proposed CodeBrain model on two public brain MRI datasets (i.e., IXI and BraTS 2023). Extensive experiments demonstrate that our CodeBrain model achieves superior imputation performance compared to four existing methods, establishing a new state of the art for unified brain MRI imputation. Codes will be released.

## 1. Introduction

Magnetic resonance imaging (MRI) is widely utilized in clinical practice due to its non-invasive capacity to distinguish between various tissue types, providing essential information for medical diagnosis and understanding brain

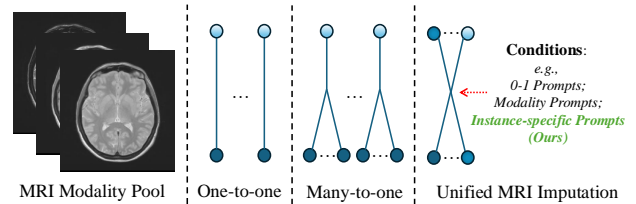


Figure 1. Illustration of different MRI imputation settings. Given multiple MRI modalities, there are various *one-to-one* and *many-to-one* transformation scenarios for synthesizing a missing one. Our proposed CodeBrain model aims to achieve a unified imputation by leveraging instance-specific prompts to generate any missing brain MRI modality.

development [13, 27, 47]. It includes a range of protocols, each producing distinct modalities that highlight specific regions of interest. For instance, T1-weighted scans are commonly used to display anatomical structures, while fluid-attenuated inversion recovery (FLAIR) scanning is a popular lesion identification tool. Additionally, contrast-enhanced modalities, such as the T1-weighted images with gadolinium (T1Gd), can further enhance abnormal regions. However, collecting a complete set of MRI modalities is often impractical, since full-modality MRI screenings are both time-consuming and costly, and the use of contrast agents may lead to potential health risks [14, 45]. Furthermore, artifacts, often arising from motion, are typically unavoidable in clinical settings, resulting in subject-level registration errors [1]. These limitations motivate the development of AI models to impute missing MRI modalities to improve clinical accessibility and diagnostic completeness.

Deep learning-based imputation models [11] have made great progress in recent years, hypothesizing that *different imaging modalities for a given subject should have similar and transformable information*. This assumption is widely supported in the medical domain [35]. For instance, pancreatic cancers can be segmented from non-contrast CT images even when they are undetectable to human experts [4]. Similarly, SynthStrip [19] and SynthSeg [2] achieve robust

Correspondence to yicheng.wu@monash.edu.

anatomical structure segmentation across different brain modalities, further suggesting structural similarity among different modalities. Consequently, restoring missing information from limited modalities in brain MRI is feasible. As illustrated in Fig. 1, prior approaches mainly focus on various *One-to-one* or *Many-to-one* synthesis scenarios, aiming to generate the desired target from a single or a set of available data. To improve synthesis performance, various techniques have been explored, including generative adversarial networks (GANs) [10, 38], diffusion models [25, 30], and transformer architectures [8, 29]. However, imputation scenarios can vary widely. For example, with four common MRI modalities (*e.g.*, T1, T2, FLAIR, and T1Gd), up to 12 one-to-one models are required to cover all possible imputation requirements. As a result, developing a unified method that can adapt to different MRI imputation scenarios is highly desirable, which can streamline clinical deployment and achieve sufficient model training by leveraging all available data.

Existing unified methods typically rely on conditional prompts to specify task targets [26, 27, 48]. For example, binary codes denote the particular imputation task setting [30]. Additionally, trainable prompts can be learned to represent various modalities, and [29] used them in a transformer architecture for unified MRI imputation. However, these approaches employing either binary or modality-specific prompts cannot fully capture the intricate variations in style and structure presented across individual samples. In addition, to reduce the inter-modality differences, other attempts such as using multiple modality-specific modules [29, 54] would limit generalization capabilities and increase computational demands. To address this, our core idea is to develop instance-specific prompts tailored to each subject’s unique imaging characteristics, to improve the accuracy and robustness of unified brain MRI imputation. On the other hand, these instance-specific prompts should remain relatively simple, since overly complex prompts would make it extremely difficult to learn transformations across diverse medical modalities and instances.

Therefore, in this paper, we proposed a new unified model, **CodeBrain**, to map each sample to instance-specific scalar-quantized codes and predict full-modality codes from incomplete inputs, enabling various inter-modality brain MRI transformations. Specifically, our CodeBrain training process consists of two stages. The first stage is to reconstruct a target modality from a source modality to learn a low-dimensional scalar-quantized code for each instance at each modality. Any target modality can be reconstructed at high quality with the corresponding code augmented with common features extracted from any other subject-level modality. Based on the constructed finite discrete code space, the second stage is to train a model to predict full-modality codes from randomly masked MRI samples, to

simulate various imputation scenarios.

Our major contributions can be summarized as follows.

- We propose a new paradigm for unified brain MRI imputation, *i.e.*, via instance-specific low-dimensional quantized codes, which is able to capture instance-level characteristics and effectively and efficiently convert the challenging modality transformation task into a full-modality code prediction task.
- We design our CodeBrain as a two-stage training framework. The first stage focuses on obtaining instance-specific scalar-quantized codes via a reconstruction process and the second stage is to predict full-modality codes using a customized grading loss.
- Extensive experiments on two datasets demonstrate our proposed CodeBrain model surpasses four existing state-of-the-art (SOTA) methods and synthesizes high-quality missing modalities, setting a new SOTA performance for unified brain MRI imputation.

## 2. Related Work

### 2.1. MRI Imputation

Data incompleteness is a prevalent challenge in large-scale medical AI applications. Considering the limited accessibility of comprehensive medical data, deep learning models have been applied to generate various missing targets [3, 11, 16, 33]. For example, [34] proposed a 3D cycle-GAN model to generate the corresponding PET from MRI to aid in Alzheimer’s disease diagnosis. An image-to-image translation model was developed in [45] to synthesize the cerebral blood volume data from standard MRI modalities, enhancing its clinical applicability.

Recent studies have focused on unified MRI imputation. For instance, MMSYN [6] proposed to learn a modality-invariant latent representation that can be decoded into different MRI modalities. MMGAN [38] employed GAN models to improve the synthesis quality. MMT [29] utilized a Swin Transformer with modality-dependent queries to generate missing modalities. M2DN [30] applied a diffusion model with binary conditional codes to specify different imputation tasks. Furthermore, [54] explored the use of modality-shared and modality-specific modules to improve unified imputation performance, and [9] incorporated federated learning for multi-modal MRI synthesis.

Nevertheless, most existing unified approaches still operate in a pixel-to-pixel inter-modality transformation scheme. In contrast, our proposed CodeBrain framework performs inter-modality transformation at the quantized latent code level and synthesizes a missing modality with the predicted code plus the extracted common features, which achieves a more robust mapping across modalities and eliminates the need for modality-specific modules.

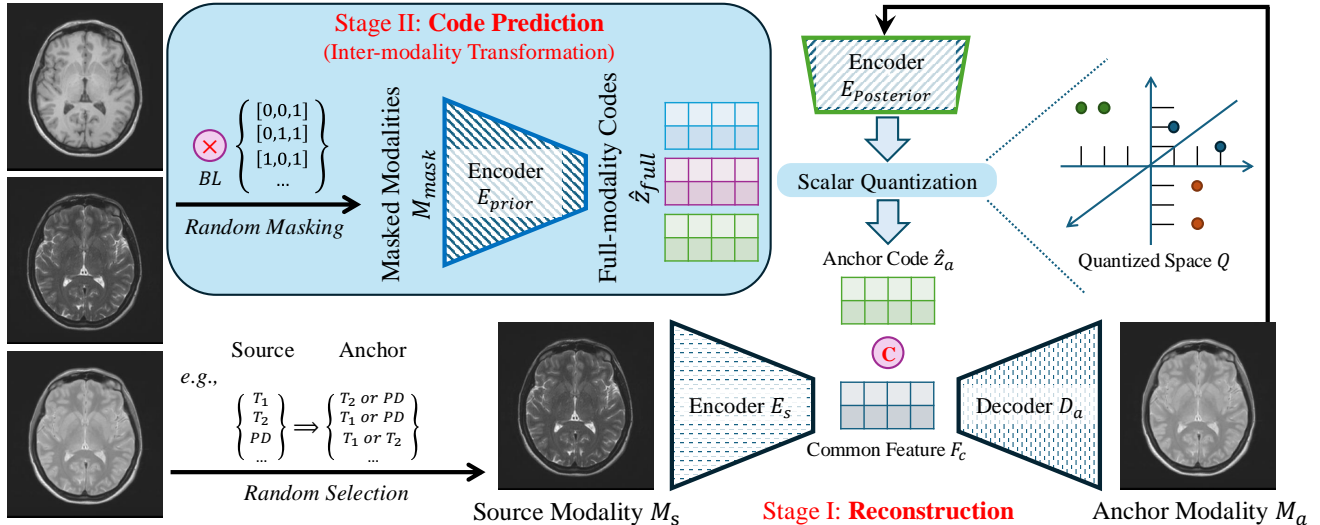


Figure 2. Pipeline of our proposed CodeBrain framework for unified Brain MRI imputation. It consists of two training stages: Stage I constructs a latent quantized space and each sample is projected to its particular scalar codes while Stage II aims to predict full-modality MRI codes with randomly masked inputs. Note that, all modules inside our CodeBrain are modality-agnostic.

## 2.2. Quantization-based Image Generation

Quantization projects complex data into a low-dimensional representation, facilitating multi-modal alignment, mapping, and fusion [18]. Data-driven vector quantization (VQ) techniques have been widely applied in image-based reconstruction, transformation, and generation tasks [12]. Solutions like the straight-through estimator (STE) [43] and Gumbel-softmax [23] are commonly used to back-propagate gradients in quantization modules, enabling end-to-end training. For example, VQVAE [43] introduced the neural discrete representation, while VQGAN [12] employed a patch GAN model to capture fine details and a transformer to predict code indices for high-resolution image synthesis. To improve the image generation quality, residual designs [28], multi-scale codebooks [36, 46], dynamic token embeddings [21], code splitting [55] have been proposed to improve VQ representation capacity. Recently, beyond region-level VQ, global quantization methods [41, 52] have been explored to disentangle multi-level visual signals. Furthermore, VQ has been incorporated with the diffusion and transformer models [15, 37, 40] to produce high-fidelity generation results.

However, training a robust codebook with high utilization is still a critical challenge in VQ-related studies [31]. Therefore, implicit codebooks have been introduced, where the decoder reconstructs targets from code indices only instead of relying on the nearest learnable code vectors [17]. For example, MAGVIT [51] introduced lookup-free quantization [5] by compressing data into binary indices, achieving superior video generation results. FSQ [31] proposed

to use scalar quantization with a straightforward rounding operation, discarding the complex process of learning an effective codebook. Following them, our proposed CodeBrain model generates scalar-quantized codes in a finite discrete space, which can be seen as instance-specific prompts and followed by the enhancement of common features to improve brain MRI reconstruction performance.

## 3. Method

Fig. 2 provides an overview of our proposed CodeBrain model. The core idea is to perform inter-modality transformations as predicting scalar-quantized codes in a latent quantized space  $Q$  while recovering any missing modality by decoding the recovered code with the extracted common feature from any available modality. Specifically, the training process consists of two stages. Stage I constructs a finite scalar space and quantizes each sample into a specific code map. Then, Stage II predicts full-modality codes from various incomplete MRI inputs, supervised by individual codes reconstructed in Stage I, to achieve a unified brain MRI imputation. During inference, given any incomplete inputs, we use the prior encoder  $E_{prior}$  to predict all modality codes. For any missing modality, we feed the corresponding predicted code, together with the common features extracted by the encoder  $E_s$ , to the decoder  $D_a$  to recover it.

### 3.1. Stage I: Reconstruction

The purpose of Stage I is to reconstruct an anchor modality  $M_a$  from a source modality  $M_s$  ( $M_s \neq M_a$ ) via an encoder ( $E_s$ ) and decoder ( $E_a$ ) architecture. The uniqueness is the design of the **bottleneck feature representation**,

which consists of a common feature extracted from  $M_s$  by  $E_s$  and an anchor code extracted from  $M_a$  by a posterior encoder  $E_{posterior}$ , aiming to capture modality-agnostic detailed information and anchor-specific coarse information respectively. Specifically, given a subject containing  $N$  distinct MRI modalities, we randomly select one modality as the source  $M_s$  and another one as the anchor  $M_a$ . Following [31], we first encode  $M_a$  into a low-dimensional latent feature  $F_a$  of size  $d \times h \times w$  by  $E_{posterior}$ , and then element-wise scalar-quantize it to  $L$  values as

$$\begin{aligned} F_a &= E_{posterior}(M_a) \\ Z_a &= \lfloor L/2 \rfloor \times \tanh(Z_a) \\ \hat{Z}_a &= Round(Z_a), \end{aligned} \quad (1)$$

where  $Z_a$  is the bounded feature and  $\hat{Z}_a$  is the scalar-quantized anchor code by the rounding operation  $Round$ . To enable end-to-end training, following STE [43],  $\hat{Z}_a$  can be represented as  $(Z_a + sg[\hat{Z}_a - Z_a])$ , where  $sg[\cdot]$  is the stop-gradient operation, essentially copying the gradients before and after  $Round$ . Note that,  $Z_a$  has  $d$  dimensions and the scalar quantization is performed for each dimension respectively. Along each dimension, there are  $L$  possible integer values, and the total possible number of quantized vectors (*i.e.*, code elements) is  $L^d$ . Additionally, each element in  $\hat{Z}_a$  indicates a quantized representation for an image patch in  $M_a$ . Such a simple scalar quantization introduced in [31] does not require learning an explicit codebook with no auxiliary losses [50] needed to regularize the training.

Since the quantization process is lossy and the code is low-dimensional, it cannot restore all details of anchor  $M_a$ . To improve the synthesis quality, we exploit a source encoder  $E_s$  to generate common features  $F_c$  from  $M_s$ . Note that  $F_c$  is modality-agnostic, which is achieved by extracting  $F_c$  from any randomly selected modality and enforcing it to contribute to any other modality. Specifically, we have

$$\begin{aligned} F_c &= E_s(M_s), \\ \tilde{M}_a &= D_a(Concat[\hat{Z}_a, F_c]) \end{aligned} \quad (2)$$

where  $\tilde{M}_a$  denotes the corresponding reconstructed results from  $D_a$  with the concatenated input of both  $\hat{Z}_a$  and  $F_c$ . Finally, we train the Stage I model with the following overall reconstruction loss:

$$\mathcal{L}_{rec} = \mathcal{L}_{psnr}(\tilde{M}_a, M_a) + \lambda \times \mathcal{L}_{gan}(\tilde{M}_a, M_a) \quad (3)$$

where  $\mathcal{L}_{psnr}$  is a differentiable loss of Peak Signal-to-Noise Ratio (PSNR) [7],  $\mathcal{L}_{gan}$  is a PatchGAN loss [22] to capture the image details, and  $\lambda$  is a hyper-parameter to balance the two terms during training.

Our Stage I designs have several advantages: 1) Different modalities are projected to a shared latent space, reducing the inter-modality gap; 2)  $\hat{Z}_a$  is instance-specific and

denotes inter-modality differences, while  $F_c$  aims to capture the modality-shared information, bridging both Stage I and Stage II; 3) The model training only relies on two losses, avoiding the complex tuning of many optimization targets.

### 3.2. Stage II: Code Prediction

Once Stage I learns instance-specific codes in the quantized space, the purpose of Stage II is to establish inter-modality transformations by directly predicting the codes of missing modalities. For Stage II training, we first concatenate different modalities along the channel dimension together to get the full-modality data  $M_{full}$  and then perform random masking by a randomly generated binary list  $BL$  to simulate various imputation scenarios. Specifically, we randomly mask  $k$  channels out of  $N$  channels/modalities of  $M_{full}$ , with  $0 < k < N$ :

$$M_{mask}^i = \begin{cases} M_{full}^i & \text{if } BL(i) = 1 \\ 0 & \text{if } BL(i) = 0 \end{cases} \quad (4)$$

where  $i$  is the channel index. Then, a prior encoder  $E_{prior}$  is trained to generate full-modality codes from the masked input  $M_{mask}$ .

The training of Stage II is supervised by  $\hat{Z}_{full}$ , a channel-wise concatenation of quantized codes of  $N$  MRI modalities from Stage I:

$$\begin{aligned} \tilde{Z}_{full} &= E_{prior}(M_{mask}) \\ \mathcal{L}_{pred} &= \mathcal{D}(\tilde{Z}_{full}, \hat{Z}_{full}) \end{aligned} \quad (5)$$

where  $\mathcal{D}$  measures the distance between  $\tilde{Z}_{full}$  and  $\hat{Z}_{full}$ . Here the target is to predict full-modality codes so that the model is trained by the imputation of missing modalities and the reconstruction of available ones at the same time, similar to [30].

Since each code dimension can only be one of the  $L$  integers, we can directly set  $\mathcal{D}$  as a  $L$ -class cross-entropy loss to train the Stage II model. However, this design ignores the clustering characteristic of the quantized space and the distances among the pre-defined  $L$  classes. Therefore, we design a grading loss for  $\mathcal{D}$ , which is defined as an ordinal binary cross-entropy loss:

$$\begin{aligned} \mathcal{L}_{pred} &= \mathcal{L}_{bce}(\tilde{B}_{full}, \hat{B}_{full}) \\ \text{s.t.}, \tilde{B}_{full} &= T(\tilde{Z}_{full}, L), \hat{B}_{full} = T(\hat{Z}_{full}, L) \end{aligned} \quad (6)$$

where  $T$  denotes a transformation from an integer value to an array of binary values of length  $(L - 1)$ , indicating the ordinal relationships for the original class labels. For example, given a class label  $y$  in the range of  $\{0, \dots, L - 1\}$ , we create  $B_y$  as:

$$B_y^j = \begin{cases} 1 & \text{if } j < y \\ 0 & \text{else} \end{cases} \quad (7)$$

where  $j, j \in \{0, \dots, L-2\}$ , is the bit index of  $B_y$ . Note that both  $\tilde{B}_{full}$  and  $\hat{B}_{full}$  are of size  $(L-1) \times d \times h \times w$ .

The advantages of our Stage II designs can be summarized as: 1) The inter-modality transformation is designed to simply predict quantized codes at the image patch level; 2) A grading loss is used to represent the smooth code distribution in the latent space; 3) All modules are modality-shared and we don't need to rely on any modality-specific module to facilitate training.

## 4. Experiments and Results

### 4.1. Datasets

We evaluated the proposed CodeBrain model on the IXI<sup>1</sup> and BraTS 2023<sup>2</sup> [32] datasets. IXI contains non-skull-stripped MRI samples from 577 healthy subjects, which were scanned from three London hospitals using three different MRI machines. Each subject contains T1, T2, and Proton Density-weighted (PD) modalities. Since these modalities are not spatially-registered, we then use ANTsPy<sup>3</sup> to register T1 and PD to T2 rigidly. Then, following [29, 30], 90 transverse brain slices are extracted from the middle of each 3D volume. We then crop these slices into a fixed size of  $256 \times 256$  and randomly select 500 subjects for training, 37 for validation, and the remaining 40 for testing.

BraTS 2023 comprises multi-site multi-parametric MRI (mpMRI) scans of brain tumor patients, including T1, T2, FLAIR, and T1Gd modalities. Each sample is skull-stripped and rigid-registered. As [29, 30], we extract the middle 80 transverse slices in our experiments, which are further cropped to a fixed size of  $240 \times 240$ . The training, validation, and testing sets include 500, 40, and 40 randomly selected subjects, respectively.

### 4.2. Implementation Details

We first normalized these MRI slices into a fixed intensity range of 0-1 by a min-max normalization, making the voxel intensities across different subjects and different modalities comparable, same as [54]. For both datasets, we set  $\lambda$  to 1, the batch size to 48,  $d$  to 7, and  $L$  as 5 as suggested in [31]. We selected the NAFNet [7] as the backbone and used the Adam optimizer with an initial learning rate (LR) of  $1e-3$ . A cosine scheduler with a minimum LR  $1e-5$  was used to tune the LR to stabilize the model training. All experiments were conducted in an identical environment for fair comparisons (Hardware:  $8 \times$  NVIDIA GeForce 4090 GPUs; Software: PyTorch: 2.1.2, CUDA: 11.8, Random Seed: 1234). We trained the CodeBrain model for 150 epochs in each stage. The total computational complexity of our Code-

Brain model is 94.85 GMACs with 96.44 M parameters. The total training time is around 36 and 42 hours on the IXI and BraTS 2023 datasets, respectively.

We use three metrics to evaluate the performance: PSNR, Structural Similarity Index (SSIM), and Mean Absolute Error (MAE). Since the MRI data has a large range of voxel intensities, we use the float type rather than the 8-bit one to calculate these metrics. The data range of PSNR is fixed to 0-1. We compare our CodeBrain with two public unified models: MMSYN [6] and MMGAN [38], and two recent methods: transformer-based MMT [29] and diffusion-based M2DN [30], where the latter two were implemented according to their works. We will release our experimental settings to establish a public benchmark for unified brain MRI imputation.

### 4.3. Imputed Results in Different Scenarios

Table 1 gives quantitative synthesis results in different settings. Overall, PD is easier to synthesize from other modalities and T2 contains more hard-to-restore details, indicating the importance of T2 examinations in clinical practice. Furthermore, different one-to-one imputation results (*i.e.*, the top of Table 1) show that T1 can be better transformed from PD than T2, while T2 and PD are highly related, as stated in [27, 29]. Fig. 3 further shows brain MRI imputation results in different scenarios on the IXI dataset. We can see that: 1) The Stage I of our CodeBrain model captures most target details for reconstruction (*i.e.*, the 2nd column in Fig. 3); 2) Our Stage II model generates accurate and plausible anatomic structures for different missing modalities in different scenarios for brain MRI.

### 4.4. Comparisons

Table 2 gives the comparison results of our model and four existing models [6, 29, 30, 38] for unified brain MRI imputation on the IXI (Top) and BraTS 2023 (Bottom) datasets. It reveals that the CodeBrain model outperforms other methods with a significant performance gain. For example, on the IXI dataset, our CodeBrain improves the PSNR value by 0.47 dB than the second-best work [29]. Besides, for various One-to-One and Many-to-One scenarios (*i.e.*, "O→O" and "M→O" in Table 2), CodeBrain achieves superior synthesis performance on both datasets. Furthermore, in "M→O" scenarios, we can set  $M_s$  as the most relevant modality to the target, for which the mean PSNR performance can be further improved by 0.25 dB on the IXI dataset, see top (.) in the last column of Table 2. Note that, the relevance between different modalities can be captured in our Stage I via a data-driven scheme, providing a new perspective to analyze the similarity of different MRI modalities. Table 2 (Bottom) further indicates our model outperforms other methods on BraTS 2023. Here, our SSIM performance is inferior to [29, 30] since CodeBrain does

<sup>1</sup><https://brain-development.org/ixi-dataset/>

<sup>2</sup><https://www.synapse.org/Synapse:syn53708126/wiki/626320>

<sup>3</sup><https://github.com/ANTsX/ANTsPy>

Table 1. Quantitative results of our CodeBrain for different brain MRI imputation scenarios on the IXI dataset. Here, CodeBrain randomly selects the source modality  $M_s$  to generate common features  $F_c$  for imputation. If selecting the most relevant modality (e.g., PD→T2) in Stage II, the performance can be further improved, as shown within parentheses (.).

Scenarios			T1			T2			PD		
T1	T2	PD	PSNR (dB) ↑	SSIM (%) ↑	MAE (×1000) ↓	PSNR (dB) ↑	SSIM (%) ↑	MAE (×1000) ↓	PSNR (dB) ↑	SSIM (%) ↑	MAE (×1000) ↓
✓			28.04	N/A	18.91	23.61	85.14	30.42	27.16	89.17	21.15
	✓		28.31	92.64	18.26	29.91	N/A		33.34	95.73	11.70
		✓		92.87			93.10	16.31		N/A	
✓	✓			N/A			N/A		32.85 (33.92)	94.89 (95.92)	12.35 (11.04)
✓		✓		N/A		29.30 (30.43)	92.04 (93.32)	17.73 (15.73)		N/A	
	✓	✓	28.61 (28.61)	93.26 (93.27)	17.63 (17.63)		N/A			N/A	
<i>mean</i>			28.32 (28.32)	92.92 (92.93)	18.27 (18.26)	27.61 (27.98)	90.10 (90.52)	21.49 (20.82)	31.12 (31.47)	93.26 (93.60)	15.07 (14.63)

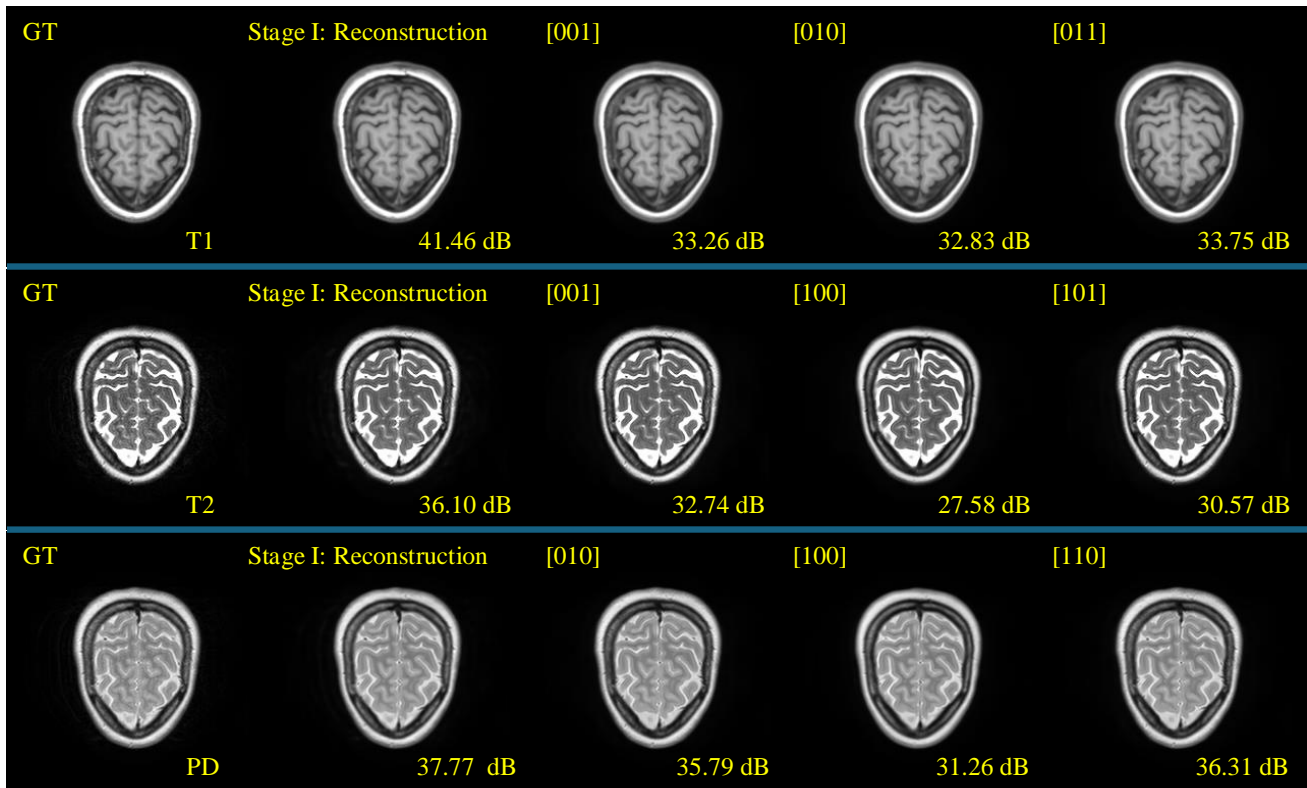


Figure 3. Exemplar synthesized brain MRI scans of our CodeBrain on the IXI dataset. There are original modalities (1st column), reconstructed results of Stage I (2nd column), and Stage II’s imputed results in different scenarios (3rd/4th/5th columns, respectively).

not involve any structure-related supervision for training and BraTS samples contain inconsistent region information (e.g., with or without clear tumor boundaries). Future work will explore structure embeddings [39] to ensure invariant anatomical representation among different modalities.

Fig. 4 provides visual comparison results on the IXI dataset. It can be seen that our model has fewer synthesis errors than other methods (e.g., the brain tissues in Fig. 4), and either the reconstruction or the imputation stage establishes a high-quality target synthesis, which is essential to reduce the scanning time and improve the feasibility of full-

modality MRI diagnosis.

#### 4.5. Ablation Studies

Table 3 gives an ablation study of our CodeBrain on the IXI dataset. In Stage I, using FSQ [31] can produce higher reconstruction performance than the original VQ [12] with the same dimension of  $d = 5$ . Increasing the code dimension to  $d = 7$  (FSQ+) improves the performance and adding common features  $F_c$  (i.e., w/  $F_c$ ) further boosts the performance by an additional 1.47 dB in PSNR. Furthermore, compared with using the traditional  $L$ -class cross-entropy loss (i.e.,

Table 2. Comparison results on the IXI (Top) and BraTS 2023 (Bottom) datasets. Here, “O→O” and “M→O” indicate one-to-one and many-to-one scenarios. As Table 1, we further show the average performance (.) by selecting the most relevant  $M_s$  on the IXI dataset.

Metrics	MMSYN [6]			MMGAN [38]			MMT [29]			M2DN [30]			Our CodeBrain		
	O→O	M→O	ALL	O→O	M→O	ALL	O→O	M→O	ALL	O→O	M→O	ALL	O→O	M→O	ALL
PSNR (dB) ↑	25.88	28.97	26.91	26.11	29.07	27.10	27.52	30.59	28.54	26.51	29.31	27.44	<b>28.40</b>	30.25 ( <b>30.98</b> )	29.01 ( <b>29.26</b> )
SSIM (%) ↑	88.96	92.90	90.27	89.11	93.05	90.42	91.03	<b>94.27</b>	92.11	89.57	92.89	90.68	<b>91.44</b>	93.40 (94.17)	92.09 ( <b>92.35</b> )
MAE (×1000) ↓	25.93	18.43	23.43	25.12	18.04	22.76	21.37	15.38	19.37	23.73	17.37	21.61	<b>19.46</b>	15.90 ( <b>14.81</b> )	18.27 ( <b>17.91</b> )
PSNR (dB) ↑	23.91	25.11	24.60	23.69	24.84	24.35	24.11	25.36	24.82	24.11	24.99	24.61	<b>24.51</b>	<b>25.46</b>	<b>25.02</b>
SSIM (%) ↑	88.75	90.38	89.69	88.03	89.88	89.09	<b>88.78</b>	90.62	89.83	<b>88.78</b>	<b>90.66</b>	<b>89.85</b>	88.40	89.64	89.09
MAE (×1000) ↓	24.81	21.34	22.83	25.02	21.90	23.24	23.79	20.48	21.90	23.79	20.98	22.22	<b>22.73</b>	<b>20.36</b>	<b>21.45</b>

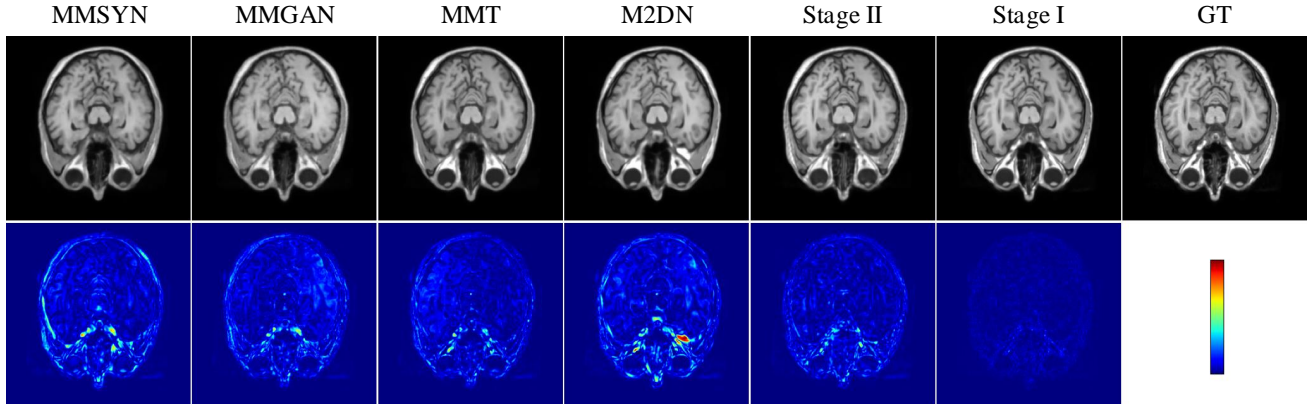


Figure 4. Comparison results on the IXI dataset in the T2→T1 scenario (Top), along with corresponding error maps (Bottom).

Table 3. Ablation studies of our CodeBrain on the IXI dataset. Here, \* and + denote the settings of  $d = 5$  and  $d = 7$  for both VQ [12] and FSQ [31] respectively, for fair comparisons.

	PSNR (dB) ↑	SSIM (%) ↑	MAE (×1000) ↓
VQ*	28.68	89.69	19.13
FSQ*	<b>32.50</b>	<b>93.51</b>	<b>12.95</b>
FSQ+	34.00	94.83	11.14
Stage I (w/ $F_c$ ) <sup>+</sup>	<b>35.47</b>	<b>96.10</b>	<b>9.22</b>
Stage II (w/ CLS)	28.61	91.48	19.15
Stage II	<b>29.01</b>	<b>92.09</b>	<b>18.27</b>

w/ CLS), the Stage II results of using our designed grading loss in (6) performs better in all the metrics. Overall, the ablation studies demonstrate the effectiveness of all the designed components in our CodeBrain model.

## 5. Discussions

### 5.1. Quantized Codes

To visualize the distributions of quantized codes in the latent space, we further show two  $32 \times 32$  code maps of our CodeBrain (#3 and #5) in Fig. 5 on the IXI dataset. We can see that, without any training regularization, the code distributions in both stages of our CodeBrain model exhibit clus-

tering characteristics. These clustered codes reflect coarse anatomical structures of the brain, potentially bridging image synthesis and perception tasks (e.g., brain segmentation [53]). Besides, the Stage II model can accurately predict most of the corresponding codes and synthesize high-quality brain MRI modalities on the IXI dataset.

### 5.2. Selection of Code Dimensions $d$

The code dimension  $d$  controls the complexity of the space  $Q$  in our CodeBrain model. Fig. 6 gives the results with different values of  $d$  on the IXI dataset. We can see that a growing  $d$  can improve the reconstruction performance (e.g., a 2.16 dB PSNR gain from  $d = 4$  to  $d = 7$ ) while the imputation performance is relatively stable (e.g., an 0.1 dB PSNR gain from  $d = 4$  to  $d = 7$ ). Therefore, we finally select  $d = 7$  to construct the quantized space on IXI.

### 5.3. Effect of Common Features $F_c$

We further investigate the reconstruction effect of extracting common features  $F_c$  from different modalities in our CodeBrain Stage I, with the results shown in Table 4. We can see that each modality can contribute to other modalities’ reconstruction and can be generated from other modalities, although with different relevance effects [27].

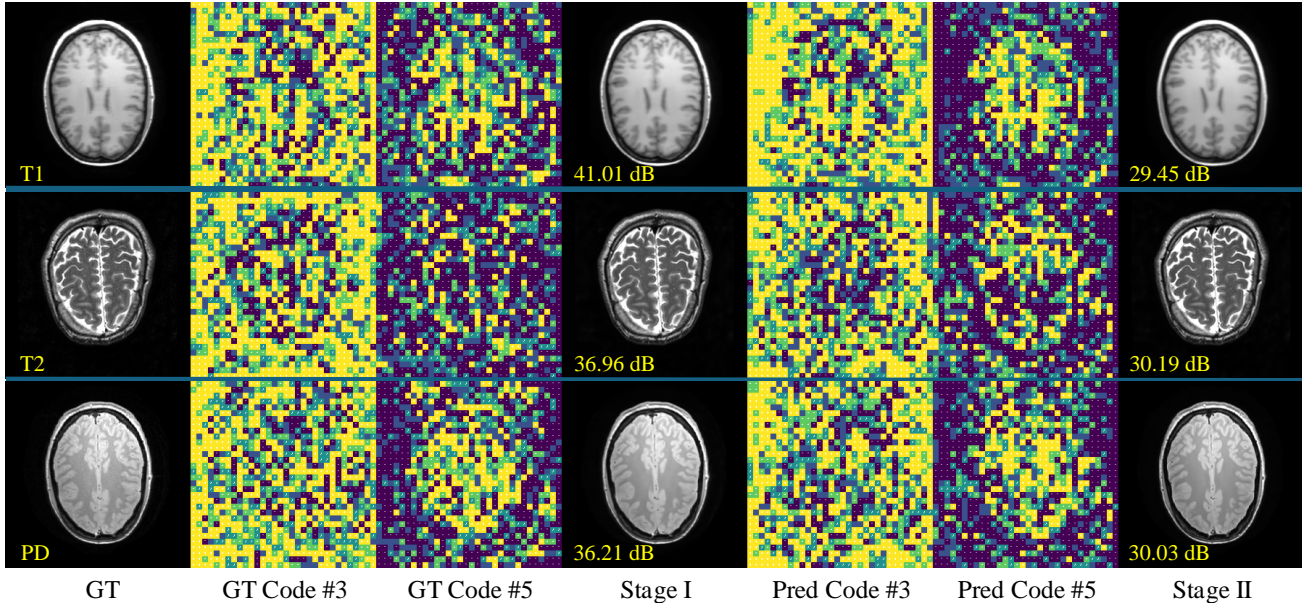


Figure 5. Exemplar  $32 \times 32$  code maps of our CodeBrain on the IXI dataset. Given  $d = 7$ , we show the 3rd and 5th channels of the codes (“M→O Scenarios”), showing clustered distributions in the latent quantized space  $Q$ .

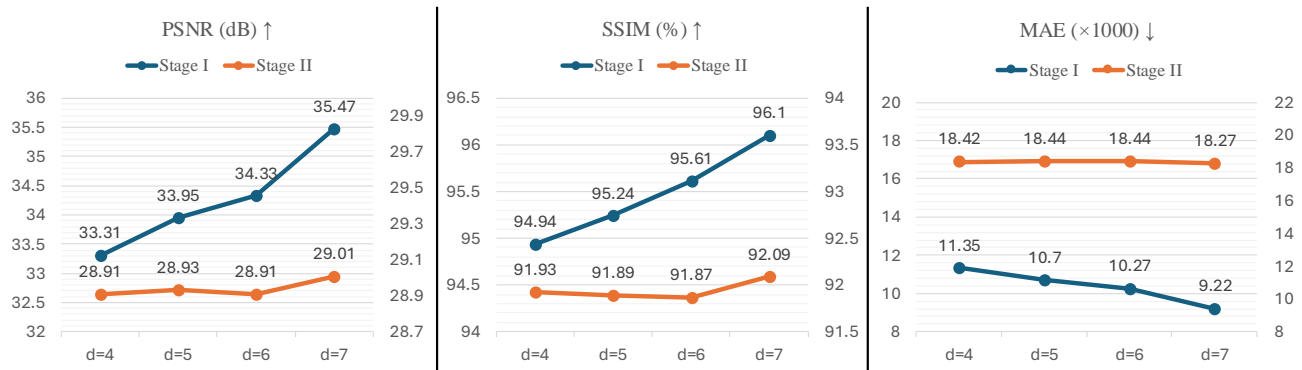


Figure 6. Quantitative results with different values of  $d$  in our CodeBrain on the IXI dataset. Here, a larger  $d$  improves the Stage I reconstruction performance, while the Stage II performance is relatively stable with different  $d$  values.

Table 4. Effect of extracting common features  $F_c$  from different modalities for the reconstruction on the IXI dataset. Performance is measured as PSNR (dB)  $\uparrow$  / SSIM (%)  $\uparrow$  / MAE ( $\times 1000$ )  $\downarrow$ .

Source \ Anchor	T1	T2	PD
T1	N/A	30.26/92.44/15.81	34.45/95.41/10.07
T2	37.81/97.98/6.67	N/A	38.46/97.33/6.89
PD	37.81/97.99/6.66	34.16/94.93/10.93	N/A

## 6. Conclusion

We have presented CodeBrain, a unified model for brain MRI imputation. The key idea is to cast the inter-modality transformation task into two stages: reconstruction and

code prediction. In the first stage, each MRI modality is compressed to a quantized code, which is augmented by common features from other modalities and then decoded to itself. In the second stage, CodeBrain predicts full-modality codes from an incomplete MRI sample. Extensive experiments on two public datasets demonstrated the effectiveness of our CodeBrain, achieving superior performance of unified brain MRI imputation.

**Limitation and Future Work.** Fig. 4 shows that despite achieving the SOTA imputation performance, our CodeBrain model still cannot fully recover the high-frequency and texture details of the original MRI scans. Further improvements could come from new estimation metrics and training losses such as those under-explored in related MRI



synthesis tasks [24, 42]. On the other hand, considering different modalities share basic priors, another direction is to explore the disentanglement [20] between the modality-shared and modality-specific information [44] from the MRI physical theory.

**Societal Impacts.** Our proposed CodeBrain model was trained and evaluated on two publicly available but limited datasets, where the dataset bias [49] may result in unconvincing predictions in clinical applications.

## References

- [1] Guha Balakrishnan, Amy Zhao, Mert R Sabuncu, John Guttag, and Adrian V Dalca. Voxelmorph: a learning framework for deformable medical image registration. *IEEE TMI*, 38(8): 1788–1800, 2019. [1](#)
- [2] Benjamin Billot, Douglas N Greve, Oula Puonti, Axel Thielscher, Koen Van Leemput, Bruce Fischl, Adrian V Dalca, Juan Eugenio Iglesias, et al. Synthseg: Segmentation of brain mri scans of any contrast and resolution without retraining. *Medical Image Analysis*, 86:102789, 2023. [1](#)
- [3] Bing Cao, Zhiwei Bi, Qinghua Hu, Han Zhang, Nannan Wang, Xinbo Gao, and Dinggang Shen. Autoencoder-driven multimodal collaborative learning for medical image synthesis. *IJCV*, 131(8):1995–2014, 2023. [2](#)
- [4] Kai Cao, Yingda Xia, Jiawen Yao, Xu Han, Lukas Lambert, Tingting Zhang, Wei Tang, Gang Jin, Hui Jiang, Xu Fang, et al. Large-scale pancreatic cancer detection via non-contrast ct and deep learning. *Nature Medicine*, 29(12): 3033–3043, 2023. [1](#)
- [5] Huiwen Chang, Han Zhang, Lu Jiang, Ce Liu, and William T Freeman. Maskgit: Masked generative image transformer. In *CVPR*, pages 11315–11325, 2022. [3](#)
- [6] Agisilaos Chartsias, Thomas Joyce, Mario Valerio Giuffrida, and Sotirios A Tsaftaris. Multimodal mr synthesis via modality-invariant latent representation. *IEEE TMI*, 37(3): 803–814, 2017. [2](#), [5](#), [7](#), [1](#)
- [7] Liangyu Chen, Xiaojie Chu, Xiangyu Zhang, and Jian Sun. Simple baselines for image restoration. In *ECCV*, pages 17–33, 2022. [4](#), [5](#)
- [8] Onat Dalmaz, Mahmut Yurt, and Tolga Çukur. Resvit: residual vision transformers for multimodal medical image synthesis. *IEEE TMI*, 41(10):2598–2614, 2022. [2](#)
- [9] Onat Dalmaz, Muhammad U Mirza, Gokberk Elmas, Muzaffer Ozbey, Salman UH Dar, Emir Ceyani, Kader K Oguz, Salman Avestimehr, and Tolga Çukur. One model to unite them all: Personalized federated learning of multi-contrast mri synthesis. *Medical Image Analysis*, 94:103121, 2024. [2](#)
- [10] Salman UH Dar, Mahmut Yurt, Levent Karacan, Aykut Erdem, Erkut Erdem, and Tolga Çukur. Image synthesis in multi-contrast mri with conditional generative adversarial networks. *IEEE TMI*, 38(10):2375–2388, 2019. [2](#)
- [11] Sanuwani Dayarathna, Kh Tohidul Islam, Sergio Uribe, Guang Yang, Munawar Hayat, and Zhaolin Chen. Deep learning based synthesis of mri, ct and pet: Review and analysis. *Medical Image Analysis*, 92:103046, 2023. [1](#), [2](#)
- [12] Patrick Esser, Robin Rombach, and Bjorn Ommer. Taming transformers for high-resolution image synthesis. In *CVPR*, pages 12873–12883, 2021. [3](#), [6](#), [7](#)
- [13] John H Gilmore, Feng Shi, Sandra L Woolson, Rebecca C Knickmeyer, Sarah J Short, Weili Lin, Hongtu Zhu, Robert M Hamer, Martin Styner, and Dinggang Shen. Longitudinal development of cortical and subcortical gray matter from birth to 2 years. *Cerebral Cortex*, 22(11):2478–2485, 2012. [1](#)
- [14] Enhao Gong, John M Pauly, Max Wintermark, and Greg Zaharchuk. Deep learning enables reduced gadolinium dose for contrast-enhanced brain mri. *Journal of Magnetic Resonance Imaging*, 48(2):330–340, 2018. [1](#)
- [15] Shuyang Gu, Dong Chen, Jianmin Bao, Fang Wen, Bo Zhang, Dongdong Chen, Lu Yuan, and Baining Guo. Vector quantized diffusion model for text-to-image synthesis. In *CVPR*, pages 10696–10706, 2022. [3](#)
- [16] Alper Güngör, Salman UH Dar, Şaban Öztürk, Yilmaz Korkmaz, Hasan A Bedel, Gokberk Elmas, Muzaffer Ozbey, and Tolga Çukur. Adaptive diffusion priors for accelerated mri reconstruction. *Medical Image Analysis*, 88:102872, 2023. [2](#)
- [17] Shaozhe Hao, Xuanton Liu, Xianbiao Qi, Shihao Zhao, Bojia Zi, Rong Xiao, Kai Han, and Kwan-Yee K Wong. Bigr: Harnessing binary latent codes for image generation and improved visual representation capabilities. *arXiv preprint arXiv:2410.14672*, 2024. [3](#)
- [18] Dailan He, Yaoyan Zheng, Baocheng Sun, Yan Wang, and Hongwei Qin. Checkerboard context model for efficient learned image compression. In *CVPR*, pages 14771–14780, 2021. [3](#)
- [19] Andrew Hoopes, Jocelyn S Mora, Adrian V Dalca, Bruce Fischl, and Malte Hoffmann. Synthstrip: skull-stripping for any brain image. *NeuroImage*, 260:119474, 2022. [1](#)
- [20] Kyle Hsu, William Dorrell, James Whittington, Jiajun Wu, and Chelsea Finn. Disentanglement via latent quantization. *NeurIPS*, 36, 2024. [9](#), [1](#)
- [21] Mengqi Huang, Zhendong Mao, Zhuowei Chen, and Yongdong Zhang. Towards accurate image coding: Improved autoregressive image generation with dynamic vector quantization. In *CVPR*, pages 22596–22605, 2023. [3](#)
- [22] Phillip Isola, Jun-Yan Zhu, Tinghui Zhou, and Alexei A Efros. Image-to-image translation with conditional adversarial networks. In *CVPR*, pages 1125–1134, 2017. [4](#)
- [23] Eric Jang, Shixiang Gu, and Ben Poole. Categorical reparameterization with gumbel-softmax. *arXiv preprint arXiv:1611.01144*, 2016. [3](#)
- [24] Liming Jiang, Bo Dai, Wayne Wu, and Chen Change Loy. Focal frequency loss for image reconstruction and synthesis. In *ICCV*, pages 13919–13929, 2021. [9](#)
- [25] Lan Jiang, Ye Mao, Xiangfeng Wang, Xi Chen, and Chao Li. Cola-diff: Conditional latent diffusion model for multimodal mri synthesis. In *MICCAI*, pages 398–408, 2023. [2](#)
- [26] Simon Kohl, Bernardino Romera-Paredes, Clemens Meyer, Jeffrey De Fauw, Joseph R Ledsam, Klaus Maier-Hein, SM Eslami, Danilo Jimenez Rezende, and Olaf Ronneberger. A probabilistic u-net for segmentation of ambiguous images. In *NeurIPS*, 2018. [2](#)

- [27] Dongwook Lee, Won-Jin Moon, and Jong Chul Ye. Assessing the importance of magnetic resonance contrasts using collaborative generative adversarial networks. *Nature Machine Intelligence*, 2(1):34–42, 2020. 1, 2, 5, 7
- [28] Doyup Lee, Chiheon Kim, Saehoon Kim, Minsu Cho, and Wook-Shin Han. Autoregressive image generation using residual quantization. In *CVPR*, pages 11523–11532, 2022. 3
- [29] Jiang Liu, Srivathsa Pasumarthi, Ben Duffy, Enhao Gong, Keshav Datta, and Greg Zaharchuk. One model to synthesize them all: Multi-contrast multi-scale transformer for missing data imputation. *IEEE TMI*, 42(9):2577–2591, 2023. 2, 5, 7, 1
- [30] Xiangxi Meng, Kaicong Sun, Jun Xu, Xuming He, and Dinggang Shen. Multi-modal modality-masked diffusion network for brain mri synthesis with random modality missing. *IEEE TMI*, 43(7):2587–2598, 2024. 2, 4, 5, 7, 1
- [31] Fabian Mentzer, David Minnen, Eirikur Agustsson, and Michael Tschanen. Finite scalar quantization: Vq-vae made simple. In *ICLR*, 2024. 3, 4, 5, 6, 7
- [32] Bjoern H Menze, Andras Jakab, Stefan Bauer, Jayashree Kalpathy-Cramer, Keyvan Farahani, Justin Kirby, Yuliya Burren, Nicole Porz, Johannes Slotboom, Roland Wiest, et al. The multimodal brain tumor image segmentation benchmark (brats). *IEEE TMI*, 34(10):1993–2024, 2014. 5
- [33] Muzaffer Özbey, Onat Dalmaz, Salman UH Dar, Hasan A Bedel, Şaban Öztürk, Alper Güngör, and Tolga Çukur. Un-supervised medical image translation with adversarial diffusion models. *IEEE TMI*, 2023. 2
- [34] Yongsheng Pan, Mingxia Liu, Chunfeng Lian, Tao Zhou, Yong Xia, and Dinggang Shen. Synthesizing missing pet from mri with cycle-consistent generative adversarial networks for alzheimer’s disease diagnosis. In *MICCAI*, pages 455–463, 2018. 2
- [35] Cheng Peng, Haofu Liao, Gina Wong, Jiebo Luo, S Kevin Zhou, and Rama Chellappa. Xraysyn: realistic view synthesis from a single radiograph through ct priors. In *AAAI*, pages 436–444, 2021. 1
- [36] Ali Razavi, Aaron Van den Oord, and Oriol Vinyals. Generating diverse high-fidelity images with vq-vae-2. *NeurIPS*, 32, 2019. 3
- [37] Robin Rombach, Andreas Blattmann, Dominik Lorenz, Patrick Esser, and Björn Ommer. High-resolution image synthesis with latent diffusion models. In *CVPR*, pages 10684–10695, 2022. 3
- [38] Anmol Sharma and Ghassan Hamarneh. Missing mri pulse sequence synthesis using multi-modal generative adversarial network. *IEEE TMI*, 39(4):1170–1183, 2019. 2, 5, 7, 1
- [39] Viswanath P Sudarshan, Shenpeng Li, Sharna D Jamadar, Gary F Egan, Suyash P Awate, and Zhaolin Chen. Incorporation of anatomical mri knowledge for enhanced mapping of brain metabolism using functional pet. *NeuroImage*, 233: 117928, 2021. 6
- [40] Haotian Tang, Yecheng Wu, Shang Yang, Enze Xie, Junsong Chen, Junyu Chen, Zhuoyang Zhang, Han Cai, Yao Lu, and Song Han. Hart: Efficient visual generation with hybrid autoregressive transformer. *arXiv preprint arXiv:2410.10812*, 2024. 3
- [41] Keyu Tian, Yi Jiang, Zehuan Yuan, Bingyue Peng, and Liwei Wang. Visual autoregressive modeling: Scalable image generation via next-scale prediction. *arXiv preprint arXiv:2404.02905*, 2024. 3
- [42] Michal R Tomaszewski and Robert J Gillies. The biological meaning of radiomic features. *Radiology*, 298(3):505–516, 2021. 9
- [43] Aaron Van Den Oord, Oriol Vinyals, et al. Neural discrete representation learning. *NeurIPS*, 30, 2017. 3, 4
- [44] Anran Wang, Jianfei Cai, Jiwen Lu, and Tat-Jen Cham. Mmss: Multi-modal sharable and specific feature learning for rgb-d object recognition. In *ICCV*, pages 1125–1133, 2015. 9, 1
- [45] Bao Wang, Yongsheng Pan, Shangchen Xu, Yi Zhang, Yang Ming, Ligang Chen, Xuejun Liu, Chengwei Wang, Yingchao Liu, and Yong Xia. Quantitative cerebral blood volume image synthesis from standard mri using image-to-image translation for brain tumors. *Radiology*, 308(2):e222471, 2023. 1, 2
- [46] Will Williams, Sam Ringer, Tom Ash, David MacLeod, Jamie Dougherty, and John Hughes. Hierarchical quantized autoencoders. *NeurIPS*, 33:4524–4535, 2020. 3
- [47] Yicheng Wu, Xiangde Luo, Zhe Xu, Xiaoqing Guo, Lie Ju, Zongyuan Ge, Wenjun Liao, and Jianfei Cai. Diversified and personalized multi-rater medical image segmentation. pages 11470–11479, 2024. 1
- [48] Yicheng Wu, Xiangde Luo, Zhe Xu, Xiaoqing Guo, Lie Ju, Zongyuan Ge, Wenjun Liao, and Jianfei Cai. Diversified and personalized multi-rater medical image segmentation. In *CVPR*, pages 11470–11479, 2024. 2
- [49] Zikang Xu, Jun Li, Qingsong Yao, Han Li, Mingyue Zhao, and S Kevin Zhou. Addressing fairness issues in deep learning-based medical image analysis: a systematic review. *npj Digital Medicine*, 7(1):286, 2024. 9
- [50] Jiahui Yu, Xin Li, Jing Yu Koh, Han Zhang, Ruoming Pang, James Qin, Alexander Ku, Yuanzhong Xu, Jason Baldridge, and Yonghui Wu. Vector-quantized image modeling with improved vqgan. In *ICLR*, 2022. 4
- [51] Lijun Yu, Yong Cheng, Kihyuk Sohn, José Lezama, Han Zhang, Huiwen Chang, Alexander G Hauptmann, Ming-Hsuan Yang, Yuan Hao, Irfan Essa, et al. Magvit: Masked generative video transformer. In *CVPR*, pages 10459–10469, 2023. 3
- [52] Qihang Yu, Mark Weber, Xueqing Deng, Xiaohui Shen, Daniel Cremers, and Liang-Chieh Chen. An image is worth 32 tokens for reconstruction and generation. *arXiv preprint arXiv:2406.07550*, 2024. 3
- [53] Wenyin Zhang, Yong Wu, Bo Yang, Shunbo Hu, Liang Wu, and Sahraoui Dhelim. Overview of multi-modal brain tumor mr image segmentation. In *Healthcare*, page 1051, 2021. 7
- [54] Yue Zhang, Chengtao Peng, Qiuli Wang, Dan Song, Kaiyan Li, and S Kevin Zhou. Unified multi-modal image synthesis for missing modality imputation. *IEEE TMI*, 2024. 2, 5
- [55] Chuanxia Zheng, Tung-Long Vuong, Jianfei Cai, and Dinh Phung. Movq: Modulating quantized vectors for high-fidelity image generation. *NeurIPS*, 35:23412–23425, 2022. 3

# CodeBrain: Impute Any Brain MRI via Instance-specific Scalar-quantized Codes

## Supplementary Material

### A. More Imputed Results on IXI

Fig. A illustrates exemplar results of our proposed CodeBrain model alongside four existing methods [6, 29, 30, 38] on the IXI dataset, evaluated under the imputation scenarios of T1→PD, T2→PD, and (T1, T2)→PD. These results demonstrate that the CodeBrain model preserves most anatomical structures and exhibits fewer synthesis errors compared to other approaches, particularly in brain tissue regions (see the 5th column in Fig. A). This observation suggests that brain tissues may share highly similar information that can be effectively quantized into low-dimensional latent representations.

Additionally, we analyzed the same subject under the T2→PD and (T1, T2)→PD scenarios (see the bottom two cases in Fig. A). The results reveal that performance improves when additional modalities are utilized for predicting the missing quantized codes in our model.

Furthermore, both Stage I and Stage II of CodeBrain consistently generate accurate PD samples across different input settings, underscoring its robust and unified brain MRI imputation capabilities on the IXI dataset.

### B. Quantitative Results on BraTS 2023

Table C gives the detailed quantitative results of our proposed CodeBrain model across various imputation scenarios on the BraTS 2023 dataset. The findings reveal: 1) The model achieves better performance in brain MRI imputation as more modalities become available; 2) Among the modalities, T1 is relatively easier to impute from other modalities, whereas FLAIR remains challenging to reconstruct; 3) Performance variations across different scenarios are not significant, suggesting that all modalities contribute similarly to the generation of other modalities on the BraTS 2023 dataset [27].

### C. Effect of Common Features on BraTS 2023

To investigate the impact of the common features  $F_c$  in our CodeBrain model, we generated  $F_c$  using different source modalities during Stage I on the BraTS 2023 dataset, as detailed in Table A. The results indicate marginal variances in performance, further suggesting that the four modalities (*i.e.*, FLAIR, T1, T2, and T1Gd) exhibit limited interdependence [27] and the common features  $F_c$  are relatively consistent across modalities within the CodeBrain framework. Here, it is noted that no additional constraints are enforced to regularize model training; instead, the model adaptively learns the common features and inter-modality transforma-

tions in a data-driven manner.

Furthermore, as shown in Table B, we conducted additional experiments by generating  $F_c$  using either a single available modality or all available modalities on the BraTS 2023 dataset. In these experiments, the source encoder  $E_s$  was identical to  $E_{prior}$  and received the masked four-channel inputs. The findings suggest that leveraging all available modalities to generate  $F_c$  leads to further performance improvements across one-to-one, many-to-one, and all imputation settings on the BraTS 2023 dataset.

Table A. Effect of extracting common features  $F_c$  from different modalities for the Stage I “reconstruction” of our CodeBrain on the BraTS 2023 dataset. Performance is measured as PSNR (dB)  $\uparrow$  / SSIM (%)  $\uparrow$  / MAE ( $\times 1000$ )  $\downarrow$ .

Source \ Anchor	FLAIR	T1	T2	T1Gd
FLAIR	N/A	36.63/97.20/5.75	34.40/97.14/6.88	33.86/95.40/7.66
T1	32.51/95.32/9.03	N/A	34.41/97.11/6.91	34.07/95.59/7.49
T2	32.60/95.50/8.89	36.72/97.29/5.69	N/A	33.92/95.48/7.60
T1Gd	32.40/95.21/9.13	36.74/97.26/5.68	34.30/97.04/6.99	N/A

Table B. Effect of using either a single available modality or all available modalities to generate the common features  $F_c$  in our CodeBrain model for unified brain MRI imputation on the BraTS 2023 dataset. When utilizing all available modalities, the source encoder  $E_s$  is designed identically to  $E_{prior}$ , with the masked four-channel input, and both stages of CodeBrain are re-trained accordingly. Additionally, O→O and M→O represent the settings for one-to-one and many-to-one imputation, respectively.

Metrics	$F_c$ (Single)			$F_c$ (All)		
	O→O	M→O	ALL	O→O	M→O	ALL
PSNR (dB) $\uparrow$	24.51	25.46	25.02	24.52	25.55	25.08
SSIM (%) $\uparrow$	88.40	89.64	89.09	88.28	89.78	89.11
MAE ( $\times 1000$ ) $\downarrow$	22.73	20.36	21.45	22.80	20.21	21.40

### D. Visual Results on BraTS 2023

Fig. B shows the reconstruction results (*i.e.*, 2nd column) and imputation outcomes under various scenarios (*i.e.*, 3rd to 9th columns) produced by our proposed CodeBrain model on the BraTS 2023 dataset. The results demonstrate that our model achieves unified brain MRI imputation while maintaining stability across different scenarios and modalities. However, despite its superior performance, the CodeBrain model struggles to capture the fine textures of the original modalities fully [20, 44]. Future work will focus on addressing this limitation to achieve high-fidelity brain MRI synthesis.

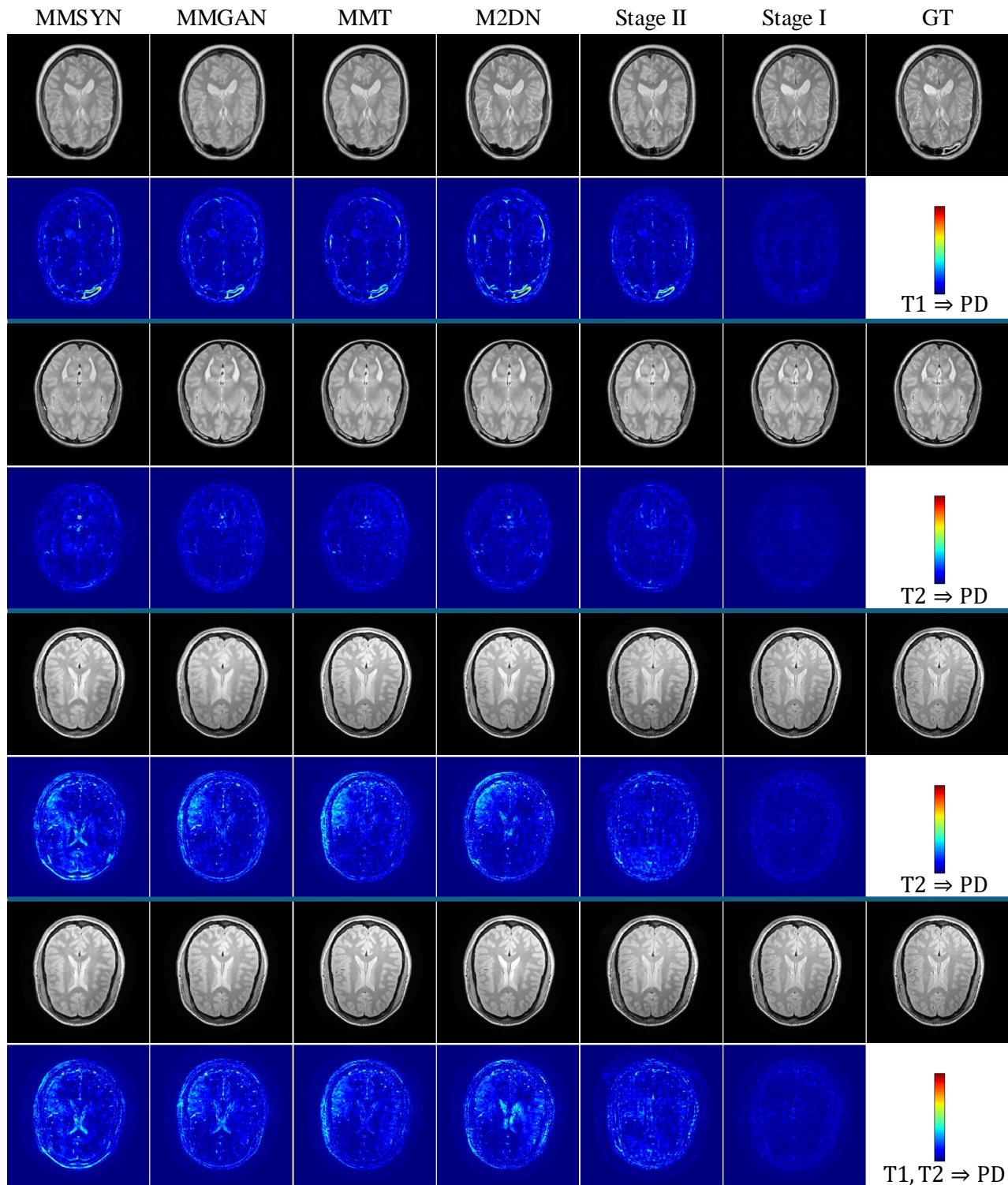


Figure A. Comparison results between our proposed CodeBrain model and four existing methods [6, 29, 30, 38] on the IXI dataset, across three brain imputation scenarios: T1 $\rightarrow$ PD (Top), T2 $\rightarrow$ PD (Middle Two Cases), and (T1, T2) $\rightarrow$ PD (Bottom), along with their corresponding error maps. Here, it clearly demonstrates that our model achieves superior brain MRI imputation, particularly in brain tissue regions (*i.e.*, 5th column). Additionally, we use the same subject's data for both T2 $\rightarrow$ PD and (T1, T2) $\rightarrow$ PD (Bottom Two Cases), highlighting that incorporating more modalities is able to further improve imputation performance in brain MRI.

Scenarios		FLAIR				T1				T2				T1Gd			
FLAIR	T1	T2	T1Gd	PSNR (dB) ↑	SSIM (%) ↑	MAE ( $\times 1000$ ) ↓	PSNR (dB) ↑	SSIM (%) ↑	MAE ( $\times 1000$ ) ↓	PSNR (dB) ↑	SSIM (%) ↑	MAE ( $\times 1000$ ) ↓	PSNR (dB) ↑	SSIM (%) ↑	MAE ( $\times 1000$ ) ↓		
√	√	√	√	23.14	N/A	26.40	25.65	89.46	20.80	23.96	89.37	23.00	23.97	85.87	24.00		
				23.58	86.35	24.42	25.96	N/A	20.10	23.88	89.57	23.62	25.32	88.01	20.16		
			√	22.93	87.81	27.02	27.25	90.70	17.33	24.03	N/A	23.14	24.44	87.31	22.77		
					85.82			91.42						N/A			
√	√	√	√	24.14	N/A	23.14	26.51	N/A	18.94	24.98	91.06	20.46	25.41	88.17	19.90		
√	√	√	√	23.40	N/A	25.62	27.69	91.17	16.54	25.18	N/A	19.99	24.75	87.54	22.03		
√	√	√	√	24.02	88.38	23.53	27.69	91.86	16.63	24.46	90.91	22.14	25.65	N/A	19.44		
					86.66			N/A						88.60			
					88.10			92.02						N/A			
√	√	√	√	23.99	N/A	23.66	27.78	N/A	16.39	25.21	N/A	19.96	25.67	88.59	19.40		
√	√	√	√		N/A			N/A			91.03			N/A			
√	√	√	√		N/A			92.08			N/A			N/A			
√	√	√	√		87.40			N/A			N/A			N/A			
				23.60	87.22	24.82	26.93	91.24	18.11	24.53	90.18	21.76	25.03	87.73	21.10		

Table C. Quantitative results of our proposed CodeBrain model for different brain MRI imputation scenarios on the BraTs 2023 dataset.

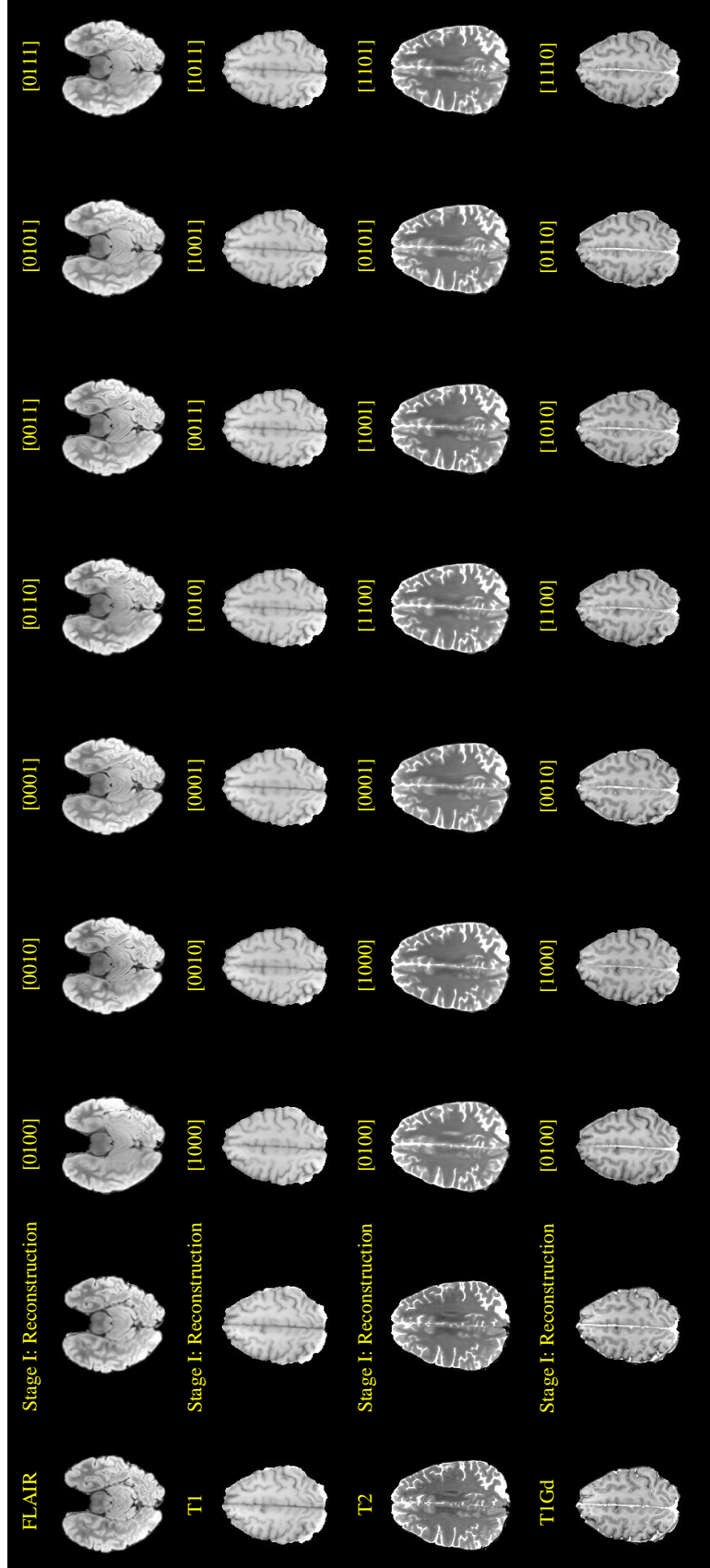


Figure B. Reconstruction (i.e., 2nd Column) and imputation results in different scenarios (i.e., 3-9 Columns) of our proposed CodeBrain model for unified brain MRI imputation on the BraTS 2023 dataset. Here, the model captures most of brain structures and the imputed results in different scenarios remain stable.